EFFECT OF CLAY STRUCTURE DEGRADATION ON SETTLEMENT OF EMBANKMENT

[2]Jidong Zhao, [1]Daichao Sheng, [1]Andrew J. Abbo, [1]Scott W. Sloan
[1]*Geotechnical Research Group, University of Newcastle, NSW 2308,* [2]*Corresponding author*

ABSTRACT

Due to the degradation of initial structures, soft clays can experience significant settlement without much change of pore pressure. Such a phenomenon has recently been observed at a fully instrumented trial highway embankment near the town of Ballina (New South Wales, Australia). In contrast, the displacements in saturated soils without structure (such as a fully remoulded clay) are always associated with the dissipation of excess pore pressure through the effective stress principle. This paper demonstrates the effects of clay structure degradation on the settlement of embankments, through numerical analysis of a trial embankment on soft clay. A constitutive model that accounts for destructuration of soils is used to characterise the behaviour of the soft clay. The material parameters are derived from conventional oedometer and triaxial tests for the structured constitutive model. It is shown that the settlement and the dissipation of excess pore pressure during construction of the embankment are closely related with the destructuration of the soft clay. With appropriate choice of the constitutive model and material parameters, the lag between the settlement and pore pressure dissipation can be well predicted by the coupled finite element method based on the effective stress principle and consolidation theory.

1 INTRODUCTION

As part of the upgrade of the Pacific Highway along the east coast of Australia, a substantial length of raised embankment is required to be constructed over areas of soft clay. Fully instrumented trial embankments have been constructed on estuarine clay deposits along the proposed alignment to acquire observational data on the settlement and stability of the highway embankments during and following the proposed construction. Extensive data on vertical settlements, lateral displacements and pore pressures have been obtained, and detailed field and laboratory tests on the clay deposits have also been carried out. This provides a useful opportunity to verify finite element codes for elastoplastic consolidation analysis, which in turn can be used to analyse the performance of the highway embankments under different design scenarios.

A distinct feature of natural soft soil that makes it behave differently from the corresponding reconstituted soil is the presence of initial structure in it. Compared to the reconstituted soil, the existence of initial structure in a natural soil may always lead to a higher void ratio. When it is subjected to loading process, the breakdown of the initial structure will lead to a destructuration process (e.g., Mitchell, 1976; Smith *et al*., 1992). This process renders the natural soil exhibiting extra strength than the corresponding reconstituted one at a given stress (Burland, 1990; Leroueil and Vaughan, 1990) and at the same time results in a significant settlement without much change of pore pressure in the soft soil. Such a phenomenon has been observed at a fully instrumented trial highway embankment near the town of Ballina (New South Wales, Australia).

Even though the Modified Cam-Clay model can be used to characterise typical behaviour in soils, like nonlinear elasticity and isotropic hardening, its deficiency in accounting for the structure in soft soils leads to the disagreement of some of its predictions with the field-monitored data as mentioned above. A specific constitutive model that is capable of addressing the initial structure and destructuration process in soft clays is thus desirable for the analysis. Fortunately, several models have been proposed to rationalise the behaviour of natural soils in literature (see e.g., Rouainia and Muir Wood, 2000; Liu *et al*., 2003; Asaoka, 2003; Baude and Stallegrass, 2004). We have successfully implemented two of them (Rouainia and Muir Wood, 2000; Asaoka, 2003) into the Newcastle Finite Element code, SNAC, and applied it to the prediction of some boundary value problems (see Zhao *et al.,* 2005).

In this paper, the model proposed by Rouainia and Muir Wood (2000) is employed to verify the settlement of the embankment by the finite element code. The model parameters are determined from a set of field and laboratory data from soft soils in Eastern Australia. Coupled analysis of deformation and pore pressure is adopted in the finite element implementation to predict the consolidation behaviours. The accuracy in settlement prediction using the consolidation theory of classical soil mechanics is also evaluated and compared with the finite element model predictions.

2 BRIEF DESCRIPTION OF THE STRUCTURE MODEL

In this section, the model proposed by Rouainia and Muir Wood (2000) that considers the structure degradation in soils is briefly described. This model has been developed to account for initial structures, small strain stiffness, stiffness degradation with strain history and hysteretic response in cyclic loading. The response associated with the elastic part in this model is expressed in terms of the bulk modulus and shear modulus, *K* and *G*, which are assumed to depend linearly on the pressure p':

$$K = \frac{dp'}{d\varepsilon_v^e} = \frac{p'}{\kappa^*}, G = \frac{3(1-2\mu)}{2(1+\mu)}K \quad \textbf{(1)}$$

where ε_v^e denotes the elastic volumetric strain; μ is the Poisson's ratio; κ^* is the slope for the swelling line in a volumetric strain-logarithmic mean stress compression plane. p' is the mean stress.

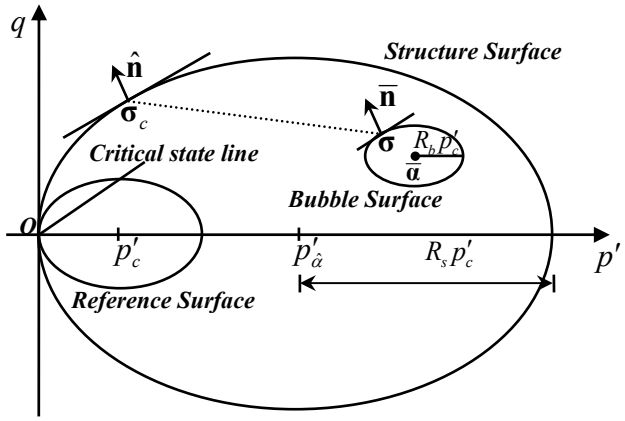

Figure 1: Illustration of yield surfaces for the structure model of Rouainia and Muir Wood (2000).

Three yield surfaces (the reference surface, the bubble and the structure surface as shown in Figure 1 are employed in this model, which, respectively, present the following analytical expressions:

$$\begin{cases} \text{Reference surface}: & f_r = g_r = \left(\dfrac{q}{M(\theta)p'_c}\right)^2 + \left(\dfrac{p'}{p'_c} - 1\right)^2 - 1 \\ \text{Bubble surface}: & f_b = g_b = \left(\dfrac{q - q_{\bar{a}}}{M(\theta)p'_c}\right)^2 + \left(\dfrac{p'}{p'_c} - \dfrac{p'_{\bar{a}}}{p'_c}\right)^2 - R_b{}^2 \\ \text{Structure surface}: & f_s = g_s = \left(\dfrac{q}{M(\theta)p'_c}\right)^2 + \left(\dfrac{p'}{p'_c} - R_s\right)^2 - R_s{}^2 \end{cases} \quad \textbf{(2)}$$

Where M denotes the slope of the critical state line (CSL), and is expressed as a function of the Lode angle θ as follows in this paper:

$$M = M_{\max}\left(\frac{2\alpha^4}{1+\alpha^4-(1-\alpha^4)\sin 3\theta}\right)^{1/4} \quad \textbf{(3)}$$

By setting the parameter α with $\alpha = (3-\sin\phi)/(3+\sin\phi)$, this yield surface coincides with the Mohr-Coulomb hexagon at all vertices in the deviatoric plane (where ϕ is the friction angle of the soil at critical state), while setting $\alpha = 1$ recovering the Von Mises circle. Note in Figure 1 that p'_c and $p'_{\hat{\alpha}}$ denote, respectively, the centres of the reference surface and structure surface; R_s and R_b denote, respectively, the initial structure and the relative ratio of the bubble size for the soft clay.

3 FINITE ELEMENT ANALYSIS

The study will focus on the data from one of the two trial highway embankments near the town of Ballina, referred to here as the *Teven Road embankment*. The alluvial and estuarine soils in the Ballina region are typical of those that prevail in coastal flood plain environments found in many parts of the East Coast of Australia. Figure 2 depicts the soil profile under the Teven Road embankment. The identified layer of silty sand (Layer 3 in Figure 2) is crucial in consolidation predictions as it will allow some degree of two-way drainage in the overlying compressible clay deposit, and at the same time it is also most susceptible to consolidation settlement. The trial embankment is 84 m long and 54 m wide at its base. A thin layer of geofabric, a 750 mm layer of fine crushed rock and a 250 mm layer of aggregate were firstly placed in an upward sequence over the entire embankment footprint and this provided a free draining surface for the underlying clay. Monitoring instruments for settlement and pore pressure were then installed over them. After covering by a further layer of geofabric, the embankment was filled gradually with ripped, weathered rock and aggregate to a maximum hight of 1.6 m over a period of 70 days (the embankment fill was placed in a stepwise manner as shown in Figure 3). The completed embankment is 44 m wide at the top.

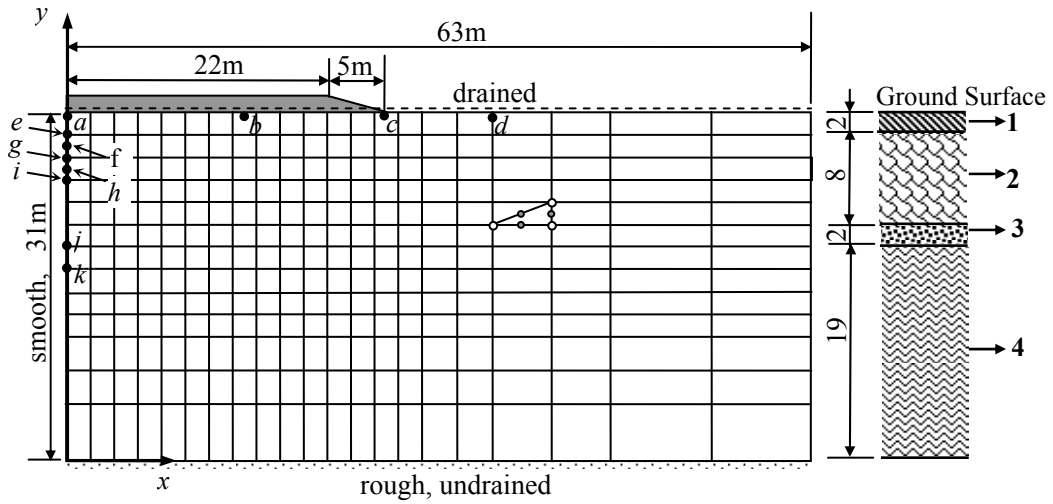

1 *Surface crust, silty CLAY, firm, brown, estuarine Lowest ground water table 1.2 m*
2 *CLAY, soft, structured, high plasticity, dark grey brown, saturated, shell fragments, estuarine*
3 *Clayey silty SAND, saturated, grey, dense, fine to medium grained*
4 *Silty CLAY, firm, dark grey, shell fragments, estuarine*

Figure 2: Typical soil profiles under the Teven Road trial embankment and the Finite element mesh for analysis (1161 nodes, 546 elements; a-k are reference points).

Figure 2 also shows the finite element mesh used to represent the soils under the embankment. Due to symmetry, only half of the embankment is considered. The embankment is represented by vertical loads which increased over time to a constant value of 30 kPa from x=0 m to x=22 m and linearly decreasing to zero from x-22 m to x=27 m. Each grid square in Figure 2 consists of two triangular elements with 6 displacement nodes and 3 pore pressure nodes. Nodes along the bottom boundary are restrained both vertically and horizontally, representing a rough boundary condition. The left and right boundaries are restrained in the horizontal directions, representing smooth contact vertically. The top boundary is set to be free drained to zero pore pressure, while the bottom boundary is set to be undrained. Four reference points on the ground surface, namely '*a'* (x=0.0 m), '*b'* (x=15.0 m), '*c'* (x=27.0 m) and '*d'* (x=34.0 m), are chosen to monitor the settlements of the trial embankment. Two other points, '*f'* (depth at 3 m or y=28.0 m) and '*h'* (depth at 5 m or y=26.0 m), are chosen to monitor the excess pore pressures. Four other reference points, '*e'*(y=29.0 m), '*g'*(y=27.0 m), '*i*' (y=25.0 m), '*j'*(y=19.0 m) and '*k'*(y=17.0 m), as shown in Figure 2, are marked for later use in FEM computations.

The experimental data, monitored from Teven Road trial embankment, are obtained by a number of triaxial tests on undisturbed samples taken from a nearby site (Robert Carr & Assoiciates Pty Ltd, 2000). These tests include consolidated undrained compression (CUC) tests, consolidated undrained extension (CUE) tests and consolidated

drained compression (CDC) tests. Appropriate optimization procedures have been used to obtain the model parameters listed in Table 1 for the finite element analysis.

Table 1: Model parameter selection optimized from the test data of Teven Road trial embankment

Layer	Depth (m)	Soil Features	λ^*	k^*	ϕ	μ	ρ	OCR	R_s	R_b	ω	A_d	B	ψ	k_p (10^{-4} m/d)
1	0~2	Desiccated clay crust	0.075	0.015	33.3°	0.20	1.81	6.65	1.0	0.1	4.0	0.9	1.8	1.4	10.2
2	2~10	Soft structured clay	0.17	0.014	33.3°	0.16	1.45	1.70	4.0	0.1	4.0	0.9	1.8	1.4	0.45
3	10~12	Clayey silty sand	0.21	0.017	33.3°	0.20	1.40	1.00	1.0	0.1	4.0	0.9	1.8	1.4	0.11
4	12-31	Firm clay	0.05	0.007	33.3°	0.20	1.62	1.06	1.0	0.1	4.0	0.9	1.8	1.4	0.25

In Table 1, λ^* and k^* denote the slopes of the Normal Compression Line (NCL) and the Unloading-Reloading Line (URL) in the plane of $\ln v - \ln p'$, respectively; ϕ is the effective frictional angle of the soil; μ and ρ are the Poisson's ratio and the density of soils, respectively; k_p is the permeability coefficient. ω, the destructuration parameter; A_d, the weight coefficient; B and ψ are, respectively, the stiffness interpolation parameter and exponent for the model (details see Rouainia and Muir Wood, 2000).

SNAC, a finite element code developed at the University of Newcastle, is used to conduct the analysis of the trial embankment. The resulting system of ordinary differential equations in term of displacement and pore pressure is treated by coupled displacement and pore pressure analysis and an adaptive time integration scheme with error control. For detailed formulation and numerical algorithms for the analysis in SNAC refer to Sloan and Abbo (1999), Sloan *et al.* (2001), Sheng and Sloan (2002) and Zhao *et al*. (2005). The initial stresses and pore pressures in the soil are generated using body loads corresponding to the bulk unit weight. Once the initial stresses are established, the initial yield surface locations are determined from the overconsolidation ratio OCR. Construction of the embankment is simulated by applying a pressure load, corresponding to the total embankment weight, over a period of 70 days. The final total weight of the embankment is 30 kPa beneath the full thickness of fill, and it is assumed to decrease linearly to zero at the toe. During the loading stage, the pore pressures at the ground surface are kept to zero and the vertical gradients of the pore pressures at 31 m depth are kept at 0 (representing an undrained boundary). The lateral boundary is taken to be impermeable. The bottom boundary at 31 m depth is fixed in both horizontal and vertical movements, representing a rough boundary. The left and right boundaries are fixed only in the horizontal movement, representing smooth boundaries in the vertical direction. After construction of the embankment, the soil layers are allowed to consolidate under the same boundary and loading conditions. The analysis is continued to a total time period of 1000 years.

4 RESULTS AND DISCUSSION

Since the construction of the embankment began, settlements and pore pressure data under the trial embankment have been measured over a 1300 day period. The predicted settlements at the ground surface and excess pore pressures at depths of 3 m and 5 m beneath the embankment centre are compared to the measured data in this section. The process of structure degradation in the soft clay will also be demonstrated.

4.1 SETTLEMENTS

The settlements at the ground surface (Reference Point *a, b, c* and *d* as in Figure 2 predicted by the finite element computation are compared against the measured data In Figure 3.

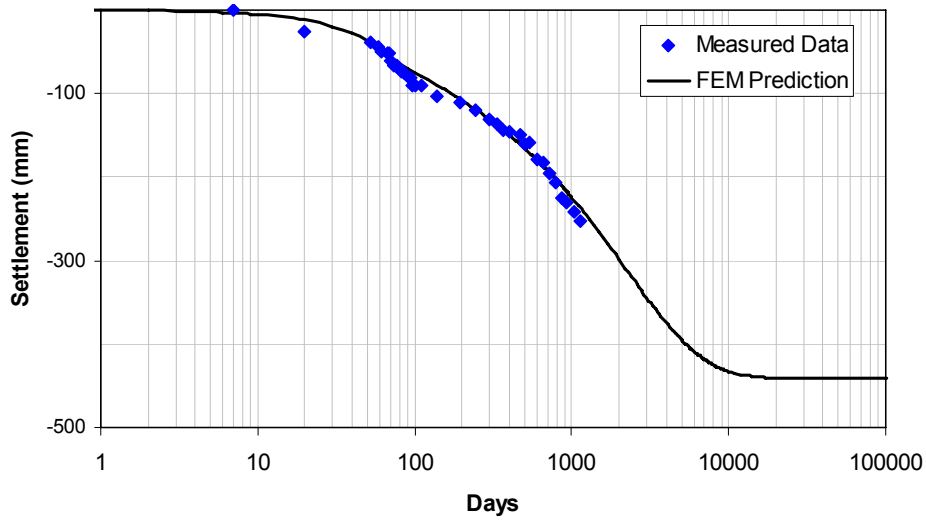

(a) Reference Point *'a'* (x=0.0 m)

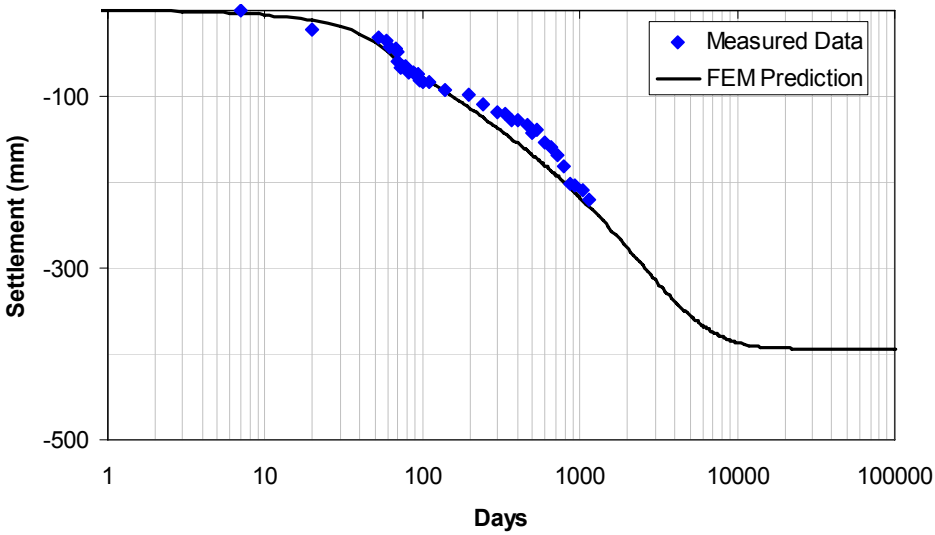

(b) Reference Point '*b*' (x=15.0 m)

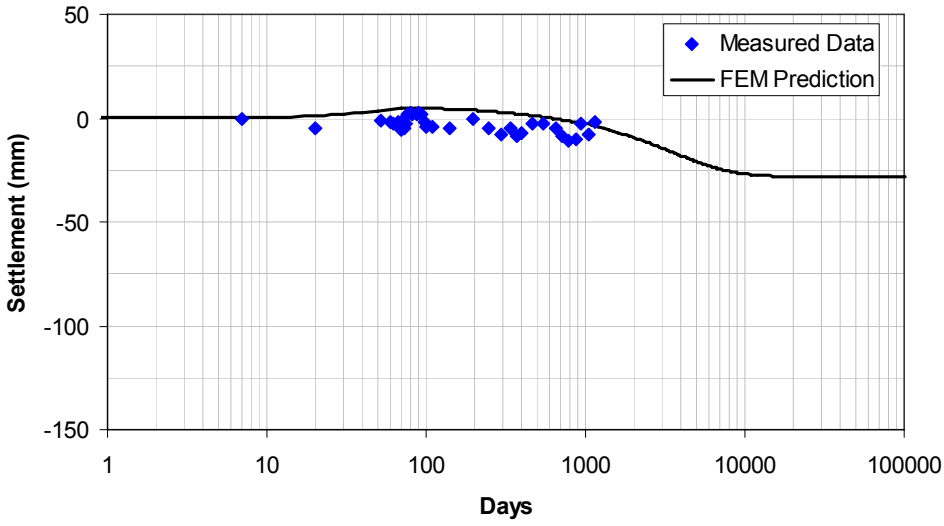

(c) Reference Point '*c*' (x=27.0 m)

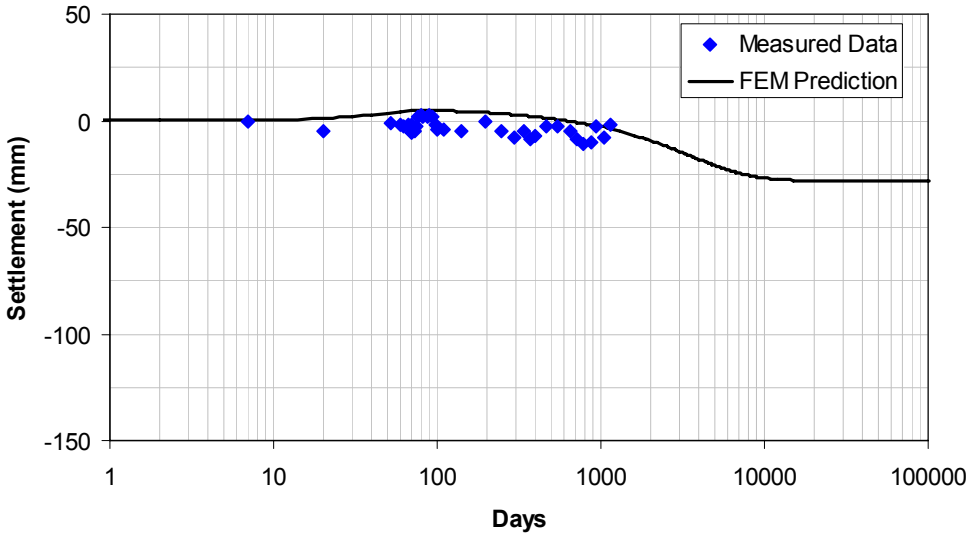

(d) Reference Point *'d'* (x=34.0 m)

Figure 3: Measured and predicted surface settlements for four reference points.

As can be seen from Figure 3(a), the finite element prediction of the time dependent settlements under the centre of the embankment (Reference Point '*a'*, x=0.0 m) agrees very well with the measured data. Only slightly smaller settlements are predicted by FEM than measured after 20 days and around 100 days. These differences are no larger than 10%. Figure 3(b) shows the ground surface settlements at the Reference Point '*b'* (x=15.0 m). The FEM predicted settlements for point '*b'* generally match well with the observed ones, except that the former underestimates the settlement up to 10% during the period between 200 days and 800 days. Figure 3(c) and Figure 3(d) depict the predicted surface settlements at the edge of the embankment (Reference Point '*c',* x=27.0 m from the centre) and outside the embankment (Reference Point '*d'*, x=34.0 m from the centre) in comparison with the observed data. The agreement between the predicted and observed responses is not as good as that shown for Reference Points *'a'* and '*b'*. The finite element method generally over-predicts the settlements at the two locations than the observed ones. Compared with the measured settlement data of Reference Points '*a'* and '*b'*, those observed at location '*c'* and '*d'* are much smaller and scattered. Thus the comparisons for '*c'* and '*d'* are not as significant as for '*a'* and '*b'*. Generally, the predicted settlements by the finite element analysis using the structure model, with parameters derived from triaxial and oedometer tests, are relatively accurate.

4.2 EXCESS PORE PRESSURE

The predicted pore pressure dissipation at depths of 3 m and 5 m beneath the embankment centre (Reference Points '*f"* and '*h'*) are compared to the measured data in Figure 4. Due to difficulties in matching the boundary condition at the ground surface, and the fluctuating ground water table in the FEM computations with the actual behaviours, the computed and measured absolute values of excess pore pressures cannot be directly compared. Thus in Figure 4 the predicted and measured excess pore pressures are normalised against their maximum values respectively, resulting in a plot of the percentages of generation and dissipation of the excess pore pressures. It is shown that the times at which the maximum excess pore pressures occur are well predicted. At about 1000 days since the construction of the embankment, around 60% of the excess pore pressure generated at a depth of 3 m has been dissipated according to the field data, while the finite element analysis predicts a dissipation of around 20%. The predicted dissipation of the excess pore pressure generated at a depth of 5 m is about 20% less than the field data at time around 1000 days. In general, compared to the settlements, the excess pore pressures predicted by the finite element method appear much less accurate, which is in accordance with those reported by Wroth and Simpson (1979).

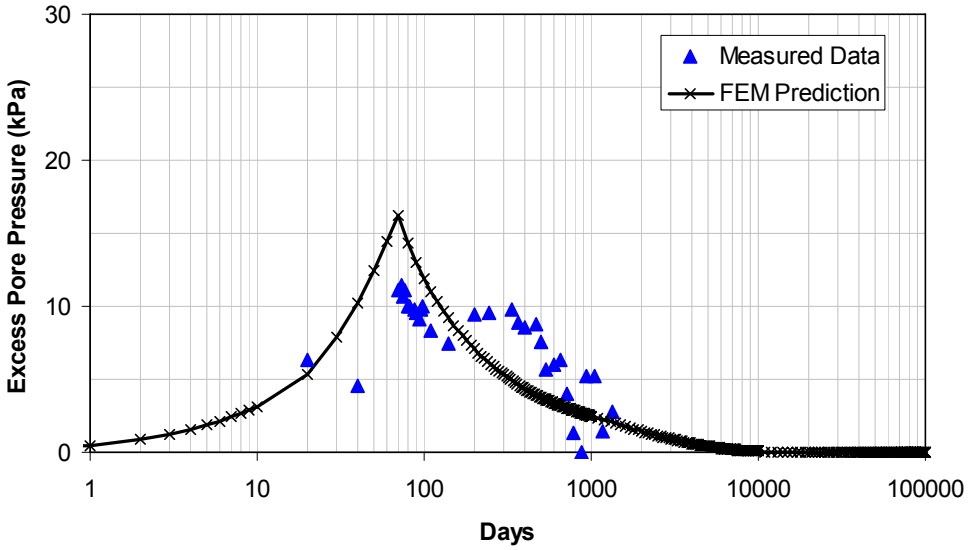

(a) Reference Point '*f*' (depth at 3 m or y=28.0 m).

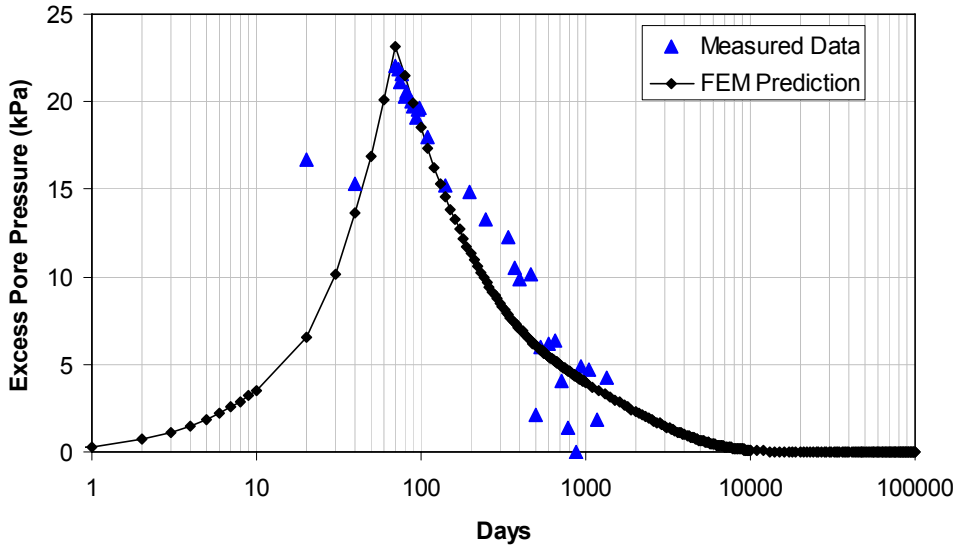

(b) Reference Point '*h*' (depth at 5 m or y=26.0 m).

Figure 4: Comparison between measured and FEM predicted excess pore water pressures beneath the centre of the embankment.

Though there are no measured data at other reference points (*e, g, i, j* and *k*) for comparison, we present the FEM predicted excess pore pressures for these points in Figure 5. As can be seen from, the peak pressures appear at around 70 days of the construction for all the reference points. And the shallower the point is the smaller the peak excess pore pressure is obtained. There is an exception, however, for points '*j*' and '*k*', as the peak pressure for '*j*' is slightly larger than that of '*k*'. This is because the reference point '*j*' is located at the boundary of the layers 3 and 4, while '*k*' is in layer 4. As it is known, layer 3 is mainly constituted of silty sand, which has very good draining properties, whereas layer 4 is composed of silty clay with poor drainage properties. Thus, on the boundary of these two layers the excess pore pressure will dissipate slower than at other places. This leads to the peak of '*j*' being higher than that of *'k'*. Another feature that may be observed from Figure 5 is, the shallower the point is, the more rapid the dissipation of excess pore pressure after peak undergoes. Comparatively, point '*e*' exhibits the most dramatic dissipation rate of excess pore pressure after the peak. On the other hand the curves after the peak for '*j*' and '*k*' show completely different features from those for *e, g* and *i.* The downward curves for *e, g* and *i* imply the dissipation rates at these locations decrease gradually over time, whereas the upward curves for '*j*' and '*k*' depict a clear increasing dissipation rate over time. However, no matter how the dissipation evolves, the excess pore pressures at all locations will decay after 10000 days.

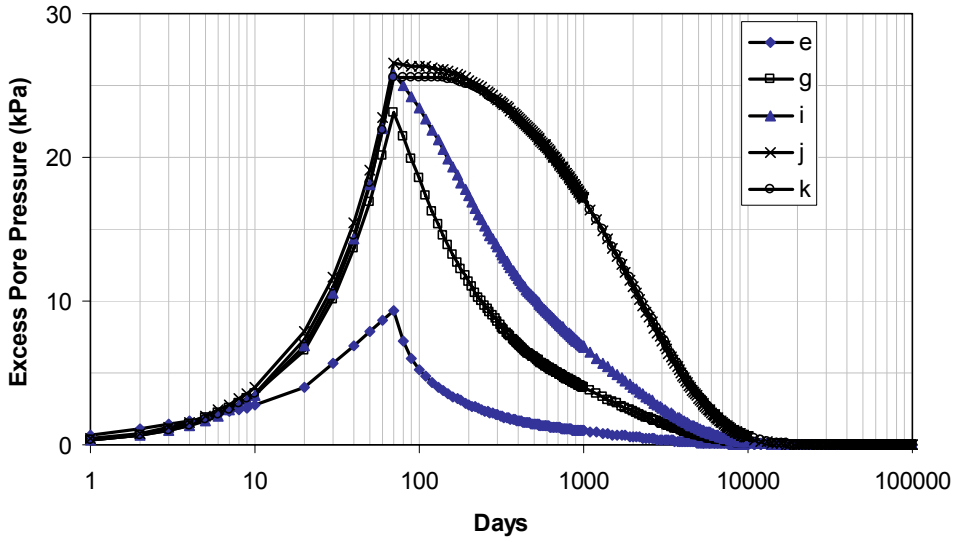

Figure 5: FEM predicted excess pore water pressures for Reference Points *e, g, i, j* and *k*.

4.3 CLAY STRUCTURE DEGRADATION

The behaviour of clay structure degradation during the embanking process can also be illustrated. The results are demonstrated in Figure 6, and observations may be made in conjunction with figure 4 and 5. As can be seen from Figure 6(a), the destructuration process is initiated just after the construction of the embankment. The shallower the point is located, the earlier this process begins. For all the four points, however, the damage caused to structure is inappreciable until 70 days of the construction. This time precisely corresponds to the point where abrupt settlements begin in Figure 3(a) and 3(b), or the point peak excess pore pressure appears in Figure 4. This coincidence is not surprising since the decay of structure in the soft clay always implies the failure of organic structure in the soil and thus leads to volumetric contractions. These volumetric contractions will unavoidably result in the settlement of ground surface of the embankment. Meanwhile, volumetric contractions will drain out water previously stored in the soil, which cause the dissipation process of excess pore pressure. Moreover, the more dramatic the decay of initial structure is, the quicker the latter two processes may be observed. Among the four points, it can be observed that the largest decay of initial structure appears earlier for the shallow points as '*f*' and '*g*' than the deeper ones as '*h*' and '*i*'. As also can be seen, none of the four points completely lose their initial structure. After 10000 days of the construction of the embankment, the structure index R_s is stable for all points and this value is greater than 1. This implies there is still some residual structure in the clay. Moreover, the points in shallow depth exhibit lower residual structure than those deeper ones.

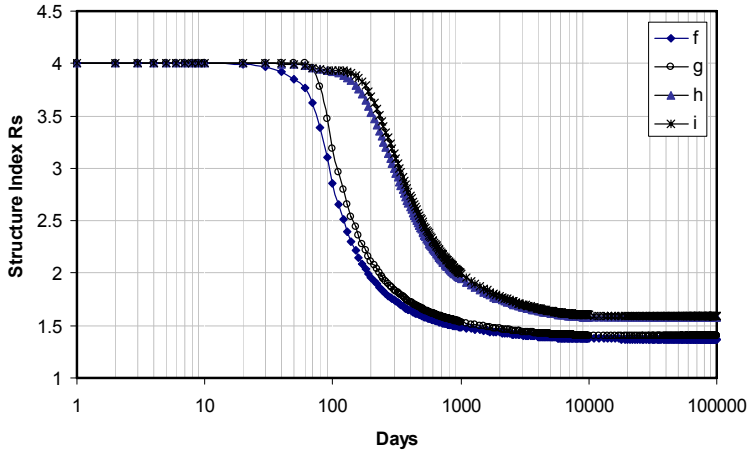

(a) Process of destructuration for Reference Points *f, g, h* and *i*.

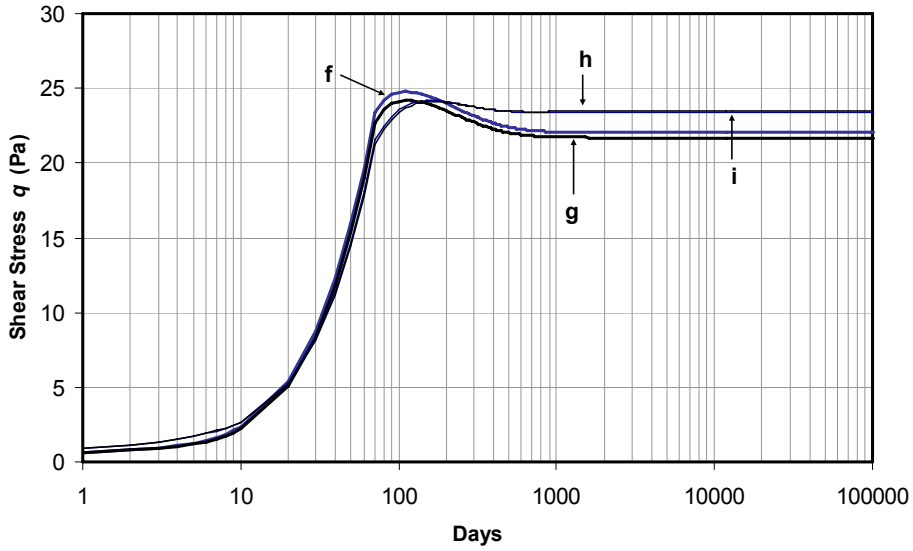

(b) Development of shear stress at Reference Points *f, g, h* and *i*.

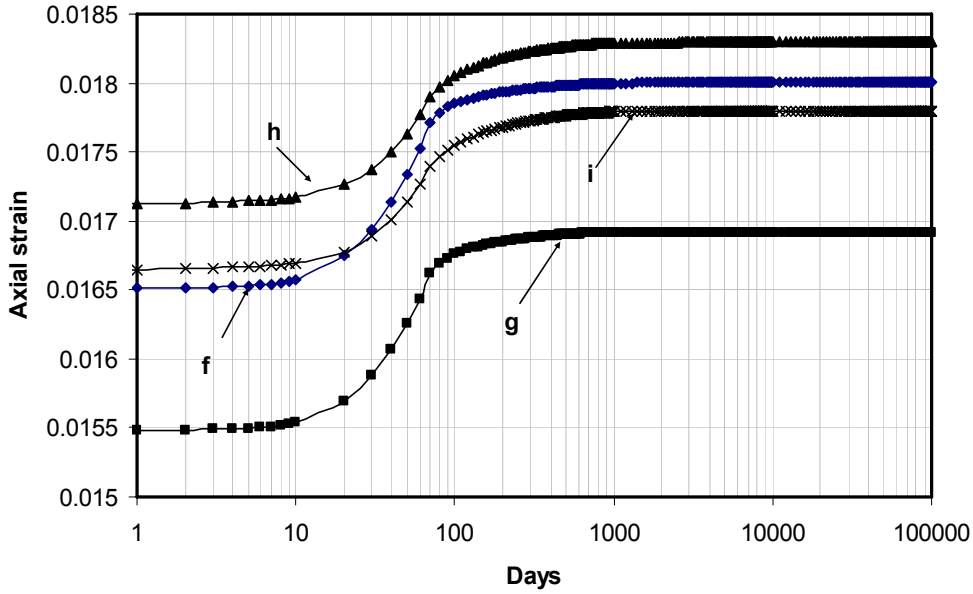

(c) Development of axial strain at Reference Points *f, g, h* and *i.*

Figure 6: Destructuration processes and stress-strain behaviour at reference points.

In Figure 6(b) and 6(c), the developments of shear stress and axial strain for the four points are depicted. In conjunction with Figure 6(a), we can observe that dramatic stress and strain increase occur before the destructuration process of the soil, which results in the accumulated plastic strain exceeding the threshold for the breakdown of the initial structure, and consequently the destructuration process is activated and the obvious decay of the initial structure in the soil is observed. This process also enables the soil to sustain some extra load, so that peak shear stress can be observed for all the four points before the stress curves go to stably horizontal.

5 CONCLUSIONS

The performance of a fully instrumented trial highway embankment on thick estuarine clay deposits is studied using the finite element method and a soil model that considers structure degradation. The performance of the numerical model in predicting the load response behaviour of soft soils found on the East Coast of Australia is evaluated. The settlements predicted by the FEM computations compare well with the data obtained from the embankment site. However, the numerical model tends to slightly under-predict the dissipation of excess pore pressure, even though the predicted rate of the settlement is relatively accurate. This discrepancy is attributed partly to the highly variable boundary conditions

in situ and partly to the inadequacy of the soil model. This paper also shows that the settlement and the dissipation of excess pore pressure are closely related to the destructuration process in soft clays. This proves the necessity of using constitutive models that take into account the effects of structure degradation to analyse geotechnical problems related to natural soft soils.

6 ACKNOWLEDGEMENTS

The authors gratefully acknowledge the provision of field and laboratory data by the Roads and Traffic Authority of New South Wales. This research was partly supported by the Australian Research Council.

7 REFERENCES

Asaoka, A. (2003) "Consolidation of clay and compaction of sand – an elastoplastic description". *12th Asian Regional Conference on SMGE*, August 2003, Singapore

Baude, B. and Stallegrass, S. (2004) "A constitutive model for structured clays". *Géotechnique* **54**(4), 269-278.

Burland, J.B. (1990) "On the compressibility and shear strength of natural clays". *Géotechnique* **40**(3), 329-378.

Leroueil, S. and Vaughan, P.R. (1990) "The general and congruent effects of structure in natural soils and weak rocks". *Géotechnique* **40**(3), 467-488.

Liu, M.D., Carter, J.P. Airey, D.W. and Liyanapathirana, D.S. (2003) "A Cam Clay-type Model for Structured Soils". *Proceedings 3rd International Symposium on the Deformation Characteristics of Geomaterials*, Lyon, France. A.A. Balkema, Lisse, Netherlands, pp1155-1160.

Mitchell, J.K. (1976). *Fundamentals of soil behaviour*. New York: John Wiley & Sons.

Robert Carr & Associates Pty Ltd, (2000). *Report on site investigation and instrumentation for the Cumbalum and Teven Road trial embankment*. Report No. 336T, Carrington, NSW, Australia

Rouainia, M. and Muir Wood, D. (2000) "A kinematic hardening constitutive model for natural clays with loss of structure". *Géotechnique* **50**(2), 152-164.

Sheng, D. and Sloan, S.W. (2003) "Time stepping schemes for coupled displacement and pore pressure analysis", *Computational Mechanics***. 31**:122-134

Sloan, S.W. and Abbo, A.J. (1999) "Biot consolidation analysis with automatic time stepping and error control, Part 1: Theory and implementation", *International Journal for Numerical and Analytical Methods in Geomechanics*, **23**, 467-492.

Sloan, S.W., Abbo, A.J. and Sheng, D. (2001) "Refined explicit integration of elastoplastic models with automatic error control", *Engineering Computations*, **18**, 121-154.

Smith, P.R., Jardine, R.J. and Hight, D.W. (1992) "The yielding of Bothkennar clay". *Géotechnique* 42(2), 257-274.

Zhao, J.D., Sheng, D.C., Rouainia, M. and Sloan, S.W. (2005) "Explicit stress integration of complex soil models". *International Journal for Numerical and Analytical Methods in Geomechanics*. **29**(12), 1209-1229.